The origin and implications of primordial helium depletion in the Afar mantle plume

Ugur Balci, Finlay Stuart, Jean-Alix Barrat, Antoniette Grima, Froukje van der Zwan

communications earth & environment | Article

https://doi.org/10.1038/s43247-024-01675-2

The origin and implications of primordial helium depletion in the Afar mantle plume

Ugur Balci[1] ✉, Finlay M. Stuart[1], Jean-Alix Barrat[2,3], Antoniette G. Grima[4] & Froukje M. van der Zwan[5]

Mantle plumes are responsible for the Earth's largest volcanic provinces. In the prevailing paradigm, the deep mantle is less degassed than convecting shallow mantle, implying that plume-derived lavas have higher concentrations of primordial volatiles such as helium (He). Demonstrating this has led to explanations that question the established Earth model. Here, we show that the ^{3}He/^{4}He of basalts from the Red Sea display coherent relationships with trace elements, allowing the helium concentration of the Afar plume to be calculated. Contrary to the prevailing model it appears the helium concentration of the Afar plume is 10-25% of the upper mantle. This contradiction is resolved if the plume material itself is a mixture of helium-rich high-^{3}He/^{4}He deep mantle with helium-depleted low-^{3}He/^{4}He recently subducted oceanic crust. This implies that helium-depleted domains may exist in convecting mantle and that moderately high ^{3}He/^{4}He plumes likely do not contain a notable contribution of the deep mantle.

Much of the Earth's intraplate volcanism is linked to deep-seated thermochemical plumes of upwelling hot mantle that originate at the core-mantle boundary[1–4]. They may originate from the margins of large low shear-velocity provinces (LLSVP) in the lower mantle[5–8] that are interpreted to be a consequence of large-scale mantle convection driven by slab subduction to the lower mantle[9–12]. Lavas from the major intraplate volcanic provinces tend to have higher ^{3}He/^{4}He ratios than lavas from mid-ocean ridges that originate in the more vigorously convecting upper mantle[13,14], while helium concentrations measured in the former ($2–17 \times 10^{-7}$ cm^3 STP/g) are notably lower than in the latter ($0.4–2.4 \times 10^{-5}$ cm^3 STP/g)[15]. The plumes with the highest flux rates, such as Iceland, Hawaii and Galapagos, have the highest ^{3}He/^{4}He[13,16,17]. Values of up to 65 R_a (where R_a is the present-day value of atmosphere of 1.34×10^{-6})[18] have been recorded in early Iceland plume basalts[19,20]. This ratio is notably higher than that of the convecting upper mantle as recorded by depleted upper mantle-derived mid-ocean ridge basalts (MORB) (8 ± 1 R_a)[21]. The relative enrichment of primordial ^{3}He in plume basalts reflects the limited degassing of the deep mantle as a consequence of mantle processing by partial melting. This evidence is corroborated by the presence of primitive Ne isotopes in high ^{3}He/^{4}He lavas from the high flux mantle plumes[22,23]. While the evidence for primordial noble gases in the deep mantle is undeniable, there is no consensus on the location of the high ^{3}He/^{4}He reservoir; explanations range from incompletely outgassed ancient mantle domains[24], the core[25] or remnants of magma ocean[26].

The prevailing models of Earth's evolution and structure require that the He concentration and ^{3}He/^{20}Ne ratio are higher in the deep mantle than in the more degassed upper mantle[13,14,27–29]. However, the absolute He concentration in high-^{3}He/^{4}He lavas is typically lower than in MORB basalts that are derived from the convecting upper mantle[15]. This long-standing helium paradox can be resolved if the deep mantle is more degassed than the upper mantle but requires that U is more incompatible in mantle melts than He[30,31]. However, the experimental determination of the partitioning of helium during melting of peridotite appears to rule out this mechanism[32]. This, along with the high partition coefficient and solubilities of the light noble gases in bridgmanite[33] and ferropericlase[34], suggests that the lower mantle should be less degassed than the upper mantle[35]. This helium paradox can also be explained if the more volatile-rich parental magmas routinely undergo disequilibrium degassing[36]. However, the extent to which this affects deep mantle-derived melts is difficult to determine. The absence of reliable estimates of the concentration of primordial volatiles in the mantle remains a major hindrance to the development of models of Earth's evolution[37].

The modern Afar mantle plume is a unique laboratory for studying the volatile inventory of the deep mantle. The Sr-Nd-Pb isotope and incompatible trace element (ITE) systematics of modern Afar mantle plume-derived basalts are well established as a mixture of three components; depleted MORB mantle, young HIMU-like plume mantle and Pan-African continental lithosphere[38,39]. Here, we report new analysis of basaltic glasses

[1]Scottish Universities Environmental Research Centre (SUERC), Rankine Avenue, East Kilbride, UK. [2]Univ Brest, CNRS, Ifremer, IRD, LEMAR, Institut Universitaire Européen de la Mer (IUEM), Place Nicolas Copernic, Plouzané, France. [3]Institut Universitaire de France, Paris, France. [4]School of Geographical and Earth Science, University of Glasgow, Glasgow, UK. [5]Earth Science and Engineering, King Abdullah University of Science and Technology (KAUST), Thuwal, Saudi Arabia. ✉e-mail: ugur.balci@glasgow.ac.uk

from a transect from the Afar mantle plume axis near the Gulf of Tadjoura along the Red Sea (Supplementary Fig. 1). They reveal coherent mixing trends between $^3He/^4He$ and ITEs. As the concentrations of trace elements in the main mantle reservoirs are well established, the mixing relationships can be used to determine the relative concentration of primordial He in the upwelling Afar mantle plume and the ambient upper mantle. The data require that the high $^3He/^4He$ mantle plume has notably lower He concentration than the upper mantle, an observation that is difficult to square with the consensus view that the deep mantle is a repository of primordial volatiles. We show how He-depleted mantle plumes can form by incorporation of subduction oceanic crust and discuss the implications.

Afar mantle plume

The earliest manifestation of the Afar mantle plume is the two-km thick sequence of continental flood basalts that covers ~400,000 km^2 in Ethiopia and Yemen formed at around 30 Ma[40]. Plume arrival triggered continental breakup and generated the Afar triple junction, resulting in the opening of Red Sea, Gulf of Aden and ongoing rifting and magmatism along the Main Ethiopian Rift (MER)[41–45]. The eruption of mid-ocean ridge basalts and the shallow Moho beneath the Red Sea and Gulf of Aden ridges imply that oceanic crust is now forming[46–48]. The absence of lithospheric mantle beneath Red Sea-Gulf of Tadjoura tends to rule it out as a contributor to the basalt chemistry and may explain why the modern Afar plume basalts have lower TiO_2 concentrations than the high $^3He/^4He$ HT2 continental flood basalts[49]. While seismic studies reveal mantle upwelling from the LLSVP at the core-mantle boundary beneath southern Africa[50–52] there is a strong low-velocity anomaly beneath the Afar region that appears to be rooted in the mantle transition zone[53–55]. The influence of the modern Afar mantle plume is evident from high $^3He/^4He$ (up to 16 R_a) and primordial Ne in basalts from Afar, the MER, southern Red Sea and Gulf of Tadjoura[23,42,56–59] and high mantle potential temperature (T_p) determined from inversion of REE concentrations (1370–1490 °C)[60,61]. The similarity of ITE and radiogenic isotope composition of the high-$^3He/^4He$ MER-Afar-Gulf of Tadjoura basalts with the earliest high Ti (HT2) lavas of the Afar CFB province (up to 21 R_a)[42,57,58,62,63] implies that the region records 30 Myr of plume-derived volcanism.

Results and discussion

Coherent $^3He/^4He$-trace element variation in Red Sea and Gulf of Tadjoura basalts

The $^3He/^4He$ of fresh basaltic glasses dredged from the Red Sea (16-26°N) and the Gulf of Tadjoura (see methods section for sample locations) show a progressive southward increase from 8.4 to 14.4 R_a (Fig. 1 and Supplementary Table 1). The $^3He/^4He$ from the northern Red Sea (8.47−8.52 R_a) overlap global MORB values[21], while high values from the Gulf of Tadjoura basalts (13.61 – 14.39 R_a) approach the highest values reported for modern basalts in the MER and Afar (15R_a)[42,57,64]. The Gulf of Tadjoura lavas have ITE and Sr, Nd and O isotopic ratios that overlap MER-Afar basalts[65–68]. Two enriched mantle components have been previously identified in Gulf of Tadjoura basalts; Tadjoura Enriched Component (TEC), which is dominated by Pan-African continental lithosphere-related, and Ramad Enriched Component (REC) that appears to be HIMU mantle thought to dominate the Afar plume[38,39]. All the glasses used in this study have Sr-Nd isotopes and trace element ratios indicating the presence of REC component[38]. Further, the trace element ratios (e.g. U/Pb, K/Nb) of the Gulf of Tadjoura basalts indicate a strong HIMU mantle signature with no evidence of notable lithosphere contribution[69]. It should be noted that the variation in Sr-Nd-Pb isotopes and the mantle heterogeneity beneath Gulf of Tadjoura revealed by previous studies[39] is not observed in basaltic glasses used in this study[38]. The Pb isotope composition of the Afar basalts is notably less radiogenic than canonical HIMU values[70], implying that the subducted oceanic crust that is present in the plume was recycled in the last few hundred Myr, a so-called "young HIMU" component[39,71–73].

The Red Sea basalts are characterised by a range of La/Sm that is indicative of two mantle components in the upper mantle north of the upwelling Afar plume[38,74]. The high $[La/Sm]_n$ (>1) (where La/Sm is normalised for primitive mantle[75]) basalts from the southern Red Sea and Gulf of Tadjoura have an enriched MORB (E-MORB) type source, while low $[La/Sm]_n$ (<1) basalts from mid- and northern Red Sea are typical of normal MORB (N-MORB)[76] (Supplementary Table 1). The heterogeneity of the mantle beneath the Red Sea is supported by the wide range in Sr-Nd-Pb isotopic composition of 13-25°N basalts ($^{87}Sr/^{86}Sr$ = 0.70240-0.70396, $^{143}Nd/^{144}Nd$ = 0.512951-0.513194, $^{206}Pb/^{204}Pb$ = 18.040-19.608)[38,77–81].

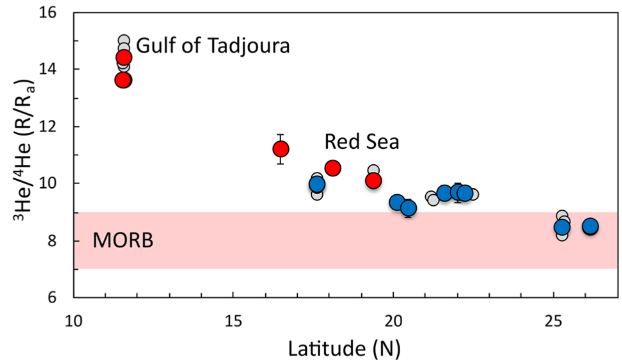

Fig. 1 | New $^3He/^4He$ ratios of 15 basaltic glass samples along the Red Sea ridge and Gulf of Tadjoura. The data can be found in Supplementary Table 1. Red circles represent E-MORB, whereas blue circles are N-MORB (see text for grouping details). Smaller grey circles represent previous data[23,56,120]. MORB $^3He/^4He$ range is 8 ± 1 R_a[21]. Error bars in the y-axis represent 1σ.

The Red Sea-Gulf of Tadjoura basalts appear to define strongly hyperbolic mixing trends when $^3He/^4He$ is plotted against a variety of ITE ratios (Fig. 2a–d). The low $^3He/^4He$ of the northern Red Sea basalts is typical of the upper asthenosphere mantle, which can be ascribed as a mixture of N-MORB and E-MORB[38], while the high $^3He/^4He$ Afar plume component defined by the Gulf of Tadjoura basalts has a strong young HIMU affinity[69].

The concentration of trace elements in young HIMU, E-MORB and N-MORB mantle end-members are determined from a generation of studies of mantle-derived basalts[75,82]. We use these constraints to infer the He concentration of the Afar plume (AP) mantle relative to the upper mantle (UM) in the Red Sea basalts. In Fig. 2, mixing lines between the high $^3He/^4He$-HIMU Afar plume mantle and the two upper mantle components using different relative helium concentrations in UM and AP ($[He]_{UM/AP}$) are shown based on the established end-member trace element concentrations (Supplementary Table 2) (see Methods section for details). The data do not define unique mixing lines; for N-MORB $[He]_{UM/AP}$ values range from 1 to 4 and for E-MORB mixing lines $[He]_{UM/AP}$ values vary from 4 to 20 (Supplementary Table 3).

The mean value determined for each sample using the four highlighted trace element ratios in N-MORB and E-MORB suggests that the Afar plume has 10-25% of the helium concentration of the local upper mantle. This is in stark contrast to the prevailing models of Earth evolution, which require that deep mantle, and therefore mantle plumes, are enriched in primordial helium relative to the degassed upper mantle[14,29,36,37,83]. The consistency of the $[He]_{UM/AP}$ values, as defined by the range of trace elements, implies that the conclusion is robust.

Helium-depleted mantle in the Afar plume

Assuming that depleted upper mantle has a maximum He concentration ($[He]_{UM}$) of 4 ×10^{14} atoms/g[28] and $[He]_{UM/AP}$ of 4-10, the upwelling Afar plume mantle has a He concentration of 0.4-1.0 ×10^{14} atoms/g. The strong young HIMU trace element signature of the Afar plume basalts implies a contribution from recycled oceanic crust (ROC)[84,85], providing a possible source of the He-depleted mantle. Within the existing paradigm, it is possible to generate a low [He]-high $^3He/^4He$ mantle by mixing primordial He-rich high $^3He/^4He$ deep mantle with He-depleted low $^3He/^4He$ recycled oceanic crust (Fig. 3). Using deep mantle $^3He/^4He$ of 65 R_a[20] and He

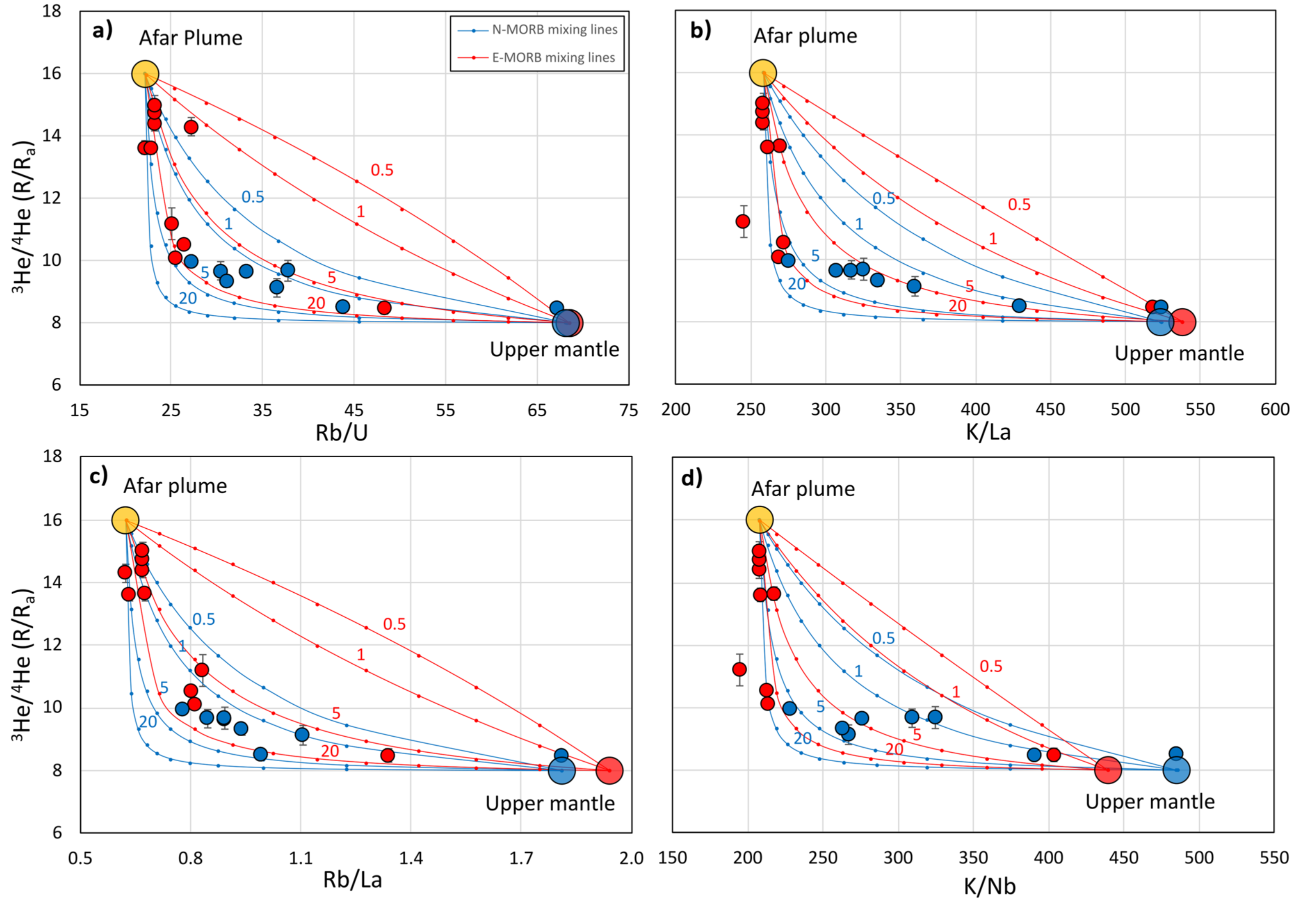

Fig. 2 | Helium isotope and trace element ratio mixing plots between Afar plume and heterogeneous upper mantle endmembers. a–d In the mixing plots, Afar plume and heterogeneous upper mantle endmembers are identified by Gulf of Tadjoura and Red Sea basalts. Trace element concentrations in the mantle endmembers are defined as; HIMU for Afar plume mantle from ref. 75; E-MORB (red circles) and N-MORB (blue circles) for the northern Red Sea[82]. The numbers above each mixing line correspond to the relative He concentrations of the upper mantle (UM) and Afar plume (AP), i.e. $[He]_{UM/AP}$. Gulf of Tadjoura samples that were previously analysed[23,56] are also shown in these plots for illustration, they were not included in the He concentration calculations (Supplementary Table 3). Error bars in the *y*-axis represent 1σ.

concentration of 1.1 $\times 10^{15}$ atoms/g[28,42], the He concentration of the ROC is in the range of $1.8-8.6 \times 10^{13}$ atoms/g for $[He]_{UM/AP}$ of 4-10 (see the example using $[He]_{UM/AP} = 4$ in Fig. 3). In this case, the He-depleted slab material dominates the Afar plume mantle (>95%). If the upwelling deep mantle in the proto-Afar plume is itself a mixture of high $^3He/^4He$ deep mantle and depleted upper mantle prior to mixing with the slab, the modern Afar plume requires a lower proportion of ROC (>85%) (Fig. 3).

Assuming that the slab was fully degassed during subduction[86,87] and it contains U and Th concentrations of ROC[88], the maximum modelled He concentration ($[He]_{max}$) of 8.6 $\times 10^{13}$ atoms/g implies that the slab was subducted within the last 80 Myr (Supplementary Fig. 2a). This is consistent with the unradiogenic Pb isotope composition of modern basalts, which contain contributions from the Afar plume ($^{206}Pb/^{204}Pb = 19.5$)[60,89]. Further, it shows that until ~1 Gyr after subduction, a downgoing slab contains less He than the deep mantle; therefore, in simple binary mixing, the deep-mantle He isotope composition will dominate (Supplementary Fig. 2b).

The best candidate for a young slab in the Afar plume is subducted Tethyan oceanic crust that has been imaged beneath the region[51,90]. Seismic tomography observations for the Afar triple junction show slow seismic velocities indicating hot upwelling mantle originating from the 660–1000 km mantle transition zone (MTZ) (SGLOBE-rani[91] in the Sub-Machine portal[92]; Supplementary Fig. 3). These profiles also track fast seismic anomalies between 440–660 km depth underlying the Zagros mountains to the north-east of the upwelling Afar plume. These fast anomalies represent the subducted Zagros-Makran slab that initiated at ~60 Ma[93,94]. Assuming the density contrast between the upper mantle and oceanic lithosphere (80 kg/m^3)[10,95,96], the mantle viscosity ratio between oceanic lithosphere to the upper mantle (50)[96,97], and the thickness of the Makran slab (70 km)[95,98], we calculate a sinking speed of 1.36 cm/year in the upper mantle for the Zagros-Makran slab (based on a simple Stokes sinker calculation – see "Methods" section). This is consistent with the global mean slab sinking rate of 1.2–1.3 cm/yr for the entire mantle[99–101]. Assuming a plume upwelling rate of 50 cm/yr[102], the slab could have subducted to no more than 1,100 km before being incorporated into the upwelling Afar plume. This implies that the Afar plume acquired its chemical and isotopic fingerprint from the Tethyan Zagros-Makran slab during large-scale mixing at the MTZ instead of the CMB. Slab-plume mixing within the MTZ and at upper lower mantle depths beneath Afar could be further facilitated by the presence of a hydrated MTZ[103,104] resulting from the continuous subduction of Tethyan slab material since Pangea break-up[51,90].

The dominance of ROC in the Afar plume mantle is consistent with the previous observation of limited deep mantle contribution (<5%) in modern Afar plume based on basalt chemistry[42]. This is difficult to reconcile with the high *Tp* recorded by MER-Afar basalts as slabs are likely to be notably colder than the deep mantle into which they are subducted[105]. It can be resolved if the dominant source of ROC in the plume is heated slab edge material. There is evidence to suggest that slab edges have a higher shear wave velocity compared to the centre of the slabs[106,107]. Slab edges are heated up to ambient mantle temperatures by the time they reach MTZ, allowing for the generation of high *Tp* readings in MER/Afar basalts[105,106].

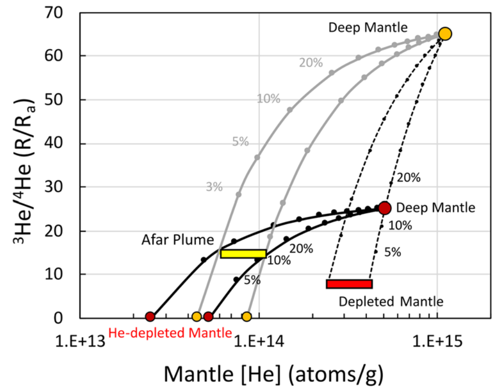

Fig. 3 | A schematic diagram of mantle He concentration and $^3He/^4He$ (R_a) illustrating how to generate the Afar plume $^3He/^4He$ signature. It displays the mixing between He-rich deep mantle and He-depleted mantle reservoirs using $[He]_{UM/AP} = 4$. Deep mantle He concentration and depleted mantle He concentration data are from refs. 28,42. The yellow rectangle represents the Afar plume generated by $[He]_{UM/AP} = 4$. The mixed deep mantle (25 R_a) can be generated by a simple mixing between the depleted mantle and deep mantle at the top of the lower mantle, represented by dashed black lines.

Implications

This study presents a reliable estimate of the absolute He content of upwelling deep mantle. In contrast to the prevailing paradigm, we find that the Afar mantle plume is depleted in primordial He relative to the convecting upper mantle. The low He content can be reconciled with the trace element and the isotopic composition of the plume lavas and can be plausibly explained by the incorporation of subducted oceanic crust in the last 80 Myr. This process generates domains of primordial volatile-depleted material. Until ~1 Gyr after subduction, downgoing slabs contain less He than the deep mantle (Supplementary Fig. 2). On this timescale, slabs can penetrate the deep mantle. Where these He-depleted mantle domains are incorporated into upwelling plumes, the bulk composition of the resulting intraplate volcanism can be dominated by the recycled slab, yet the He inventory will be dominated by the deep mantle contribution. This explains why high $^3He/^4He$ are recorded by many OIBs that display enriched geochemical signatures[13] and requires care should be exercised when using moderately high $^3He/^4He$ mantle plumes to extrapolate the bulk composition of deep Earth.

Methods

Sample collection

This study uses fresh basaltic glass samples from two young Mid-ocean ridges: Red Sea (from 26-16°N) and Gulf of Tadjoura, Republic of Djibouti (Supplementary Fig. 1). Helium isotope analysis was performed on basaltic glasses dredged from the Red Sea during R/V Poseion P408-1 (the FS Poseidon Fahrtbericht/Cruise Report P408 [POS408] from ref. 108) and R/V Pelagia 64/PE350/351 (RV PELAGIA Cruise Report 64PE350/64PE351 from ref. 109) expeditions and cruises M31/2 from ref. 110, and SO29 from refs. 23,111. The location and trace element composition of the Red Sea basalts can be found in ref. 74. The location of basalt samples dredged from the Gulf of Tadjoura can be found in ref. 38. The trace element composition of these samples were reported using the method of ref. 38 (Supplementary Table 4).

Analysis procedures: helium isotope measurements

The helium isotope composition of fifteen Red Sea-Gulf of Tadjoura basaltic glasses were measured in the SUERC noble gas laboratory (Supplementary Table 1). Ten samples were analysed using a MAP-215-50 noble gas mass spectrometer using procedures reported by ref. 112. Five samples were analysed using Helix SFT noble gas mass spectrometer following procedures reported by ref. 113. In all cases the volatiles were extracted from vesicles in basaltic glasses by *in vacuo* crushing using a multi-sample hydraulic crusher apparatus. Helium blanks during both analytical sessions were less than 1% of measured ^4He signals. Mass spectrometers were calibrated using HESJ He isotope standard.

Calculating relative mantle helium concentrations

In Fig. 2 we plot the He isotope composition of Red Sea basalts against trace element ratios. Mixing lines are plotted between Afar mantle plume and two upper mantle (N-MORB and E-MORB) components using the mass balance equations of Langmuir et al. [114]. The helium isotope ratios composition of the Afar plume (AP) is 16 R_a[42,59,60,68] and 8 R_a[21] for the upper mantle (UM) end-members. There is less clarity on the ITE ratios of the upper mantle as they reflect the source and degree of enrichment[84,115,116]. In order to accommodate the established heterogeneity in shallow mantle beneath Red Sea[38], we define end-member values for N-MORB and E-MORB mantle domains using the highest ratio recorded in samples along Red Sea[74]. For the Afar plume end-member we use the lowest ratio recorded in Gulf of Tadjoura samples according to the $[La/Sm]_n$ grouping (Supplementary Table 1). The mixing lines developed in Fig. 2 are set for $[He]_{UM/AP}$ of 0.5, 1, 5 and 20. The relative proportion of He in the mantle domains ($[He]_{UM/AP}$) has been calculated for each sample and all trace element ratios (Rb/La, Rb/U, K/La, and K/Nb) (Fig. 2 and Supplementary Table 3) using the best fit of mixing lines for each sample by changing the $[He]_{UM/AP}$ value. The mean of the samples $[He]_{UM/AP}$ value is 7 ± 3 (1σ).

Slab sinking speed V_{stoke} calculation of Makran Slab

We use Stokes law[117] to calculate the slab sinking speed $V_{Stokes,}$ of the Zagros-Makran subduction. This method assumes a simple Stokes sinker[11,118,119], which accepts a higher-density blob (slab) sinking through a viscous fluid (mantle) and calculates the speed of this sphere (Stokes sphere) to calculate the speed that the Zagros-Makran slab has been sinking;

$$V_{Stokes} = C\frac{\Delta\rho g \alpha^2}{\eta_m}; \text{where} \quad (1)$$

$$C = \frac{2 + 2\eta'}{6 + 9\eta'}; \text{where} \quad (2)$$

$$\eta' = \frac{\eta_s}{\eta_m} \quad (3)$$

Where $\Delta\rho$ is the density contrast between slab and mantle and has a value of 80 kg/m³ from refs. 10,95,96, η' is the mantle viscosity ratio between oceanic lithosphere to upper mantle with a value of 50 from refs. 96,97, α is the radius of the slablet with a value of 35,000 m after the thickness of the Makran slab taken to be 70 km from refs. 95,98. η_m is the upper mantle viscosity with a value of 5×10^{20} Pa s from ref. 97 and η_s as the oceanic lithosphere viscosity of 2.5×10^{22} Pa s from ref. 96 and g is the gravitational force taken as 9.81 m/s².

Data availability

All data analysed or generated in this study are publicly available in Figshare at https://doi.org/10.6084/m9.figshare.26517178.v1.

Received: 24 May 2024; Accepted: 3 September 2024;
Published online: 25 September 2024

References

1. Thorne, M. S., Garnero, E. J. & Grand, S. P. Geographic correlation between hot spots and deep mantle lateral shear-wave velocity gradients. *Phys. Earth Planet. Inter.* **146**, 47–63 (2004).
2. Boschi, L., Becker, T. W. & Steinberger, B. Mantle plumes: dynamic models and seismic images. *Geochem. Geophys. Geosyst.* **8**, 2–6 (2007).
3. Davies, D. R., Goes, S. & Sambridge, M. On the relationship between volcanic hotspot locations, the reconstructed eruption sites of large igneous provinces and deep mantle seismic structure. *Earth Planet Sci. Lett.* **411**, 121–130 (2015).
4. Morgan, W. J. Convection plumes in the lower mantle. *Nature* **230**, 42–43 (1971).
5. Burke, K. & Torsvik, T. H. Derivation of Large Igneous Provinces of the past 200 million years from long-term heterogeneities in the deep mantle. *Earth Planet. Sci. Lett.* **227**, 531–538 (2004).

6. Thorne, M. S., Garnero, E. J., Jahnke, G., Igel, H. & McNamara, A. K. Mega ultra low velocity zone and mantle flow. *Earth Planet. Sci. Lett.* **364**, 59–67 (2013).
7. French, S. W. & Romanowicz, B. Broad plumes rooted at the base of the Earth's mantle beneath major hotspots. *Nature* **525**, 95–99 (2015).
8. Steinberger, B. & Torsvik, T. H. A geodynamic model of plumes from the margins of Large Low Shear Velocity Provinces. *Geochem. Geophys. Geosyst.* **13**, 9–14 (2012).
9. van der Meer, D. G., van Hinsbergen, D. J. J. & Spakman, W. Atlas of the underworld: Slab remnants in the mantle, their sinking history, and a new outlook on lower mantle viscosity. *Tectonophysics* **723**, 309–448 (2018).
10. Ricard, Y., Richards, M., Lithgow-Bertelloni, C. & Le Stunff, Y. A geodynamic model of mantle density heterogeneity. *J. Geophys. Res.* **98**, 895–909 (1993).
11. Lithgow-Bertelloni, C. & Richards, M. A. The dynamics of cenozoic and mesozoic plate motions. *Rev. Geophys.* **36**, 27–78 (1998).
12. Koppers, A. A. P. et al. Mantle plumes and their role in Earth processes. *Nat. Rev. Earth Environ.* **2**, 382–401 (2021).
13. Kurz, M. D., Jenkins, W. J. & Hart, S. R. Helium isotopic systematics of oceanic islands and mantle heterogeneity. *Nature* **297**, 43–47 (1982).
14. Allègre, C. J., Staudacher, T., Sarda, P. & Kurz, M. Constraints on evolution of Earth's mantle from rare gas systematics. *Nature* **303**, 2–6 (1983).
15. Fisher, D. E. Noble gases from oceanic island basalts do not require an undepleted mantle source. *Nature* **316**, 716–718 (1985).
16. Kurz, M. D. & Geist, D. Dynamics of the Galapagos hotspot from helium isotope geochemistry. *Geochim. Cosmochim. Acta* **63**, 4139–4156 (1999).
17. Macpherson, C. G., Hilton, D. R., Day, J. M. D., Lowry, D. & Grönvold, K. High-3He/4He, depleted mantle and low-δ 18O, recycled oceanic lithosphere in the source of central Iceland magmatism. *Earth Planet Sci. Lett.* **233**, 411–427 (2005).
18. Mishima, K. et al. Accurate determination of the absolute 3He/4He ratio of a synthesized helium standard gas (Helium Standard of Japan, HESJ): toward revision of the atmospheric 3He/4He ratio. *Geochem. Geophys. Geosyst.* **19**, 3995–4005 (2018).
19. Stuart, F. M., Lass-Evans, S., Fitton, J. G. & Ellam, R. M. High 3He/4He ratios in picritic basalts from Baffin Island and the role of a mixed reservoir in mantle plumes. *Nature* **424**, 57–59 (2003).
20. Horton, F. et al. Highest terrestrial 3He/4He credibly from the core. *Nature* **623**, 90–94 (2023).
21. Graham, D. W. Noble gas isotope geochemistry of mid-ocean ridge and ocean island basalts: characterization of mantle source reservoirs. *Rev. Mineral Geochem.* **47**, 247–317 (2002).
22. Honda, M., McDougall, I., Patterson, D. B., Doulgeris, A. & Clague, D. A. Possible solar noble-gas component in Hawaiian basalts. *Nature* **349**, 149–151 (1991).
23. Moreira, M., Valbracht, P. J., Staudacher, T. & Allègre, C. J. Rare gas systematics in Red Sea ridge basalts. *Geophys. Res. Lett.* **23**, 2453–2456 (1996).
24. Mukhopadhyay, S. Early differentiation and volatile accretion recorded in deep-mantle neon and xenon. *Nature* **486**, 101–104 (2012).
25. Porcelli, D. & Halliday, A. N. The core as a possible source of mantle helium. *Earth Planet Sci. Lett.* **192**, 45–56 (2001).
26. Ozgurel, O. & Caracas, R. The magma ocean was a huge helium reservoir in the early Earth. *Geochem. Perspect. Lett.* **25**, 46–50 (2023).
27. Allègre, C. J., Staudacher, T. & Sarda, P. Rare gas systematics: formation of the atmosphere, evolution and structure of the Earth's mantle. *Earth Planet Sci. Lett.* **81**, 127–150 (1987).
28. Porcelli, D. & Wasserburg, G. J. Mass transfer of helium, neon, argon, and xenon through a steady-state upper mantle. *Geochim. Cosmochim. Acta* **59**, 4921–4937 (1995).
29. Gonnermann, H. M. & Mukhopadhyay, S. Preserving noble gases in a convecting mantle. *Nature* **459**, 560–563 (2009).
30. Anderson, D. L. The helium paradoxes. *Proc. Natl Acad. Sci. USA* **95**, 4822–4827 (1998).
31. Parman, S. W., Kurz, M. D., Hart, S. R. & Grove, T. L. Helium solubility in olivine and implications for high 3He/ 4He in ocean island basalts. *Nature* **437**, 1140–1143 (2005).
32. Jackson, C. R. M., Parman, S. W., Kelley, S. P. & Cooper, R. F. Constraints on light noble partitioning at the conditions of spinel-peridotite melting. *Earth Planet Sci. Lett.* **384**, 178–187 (2013).
33. Shcheka, S. S. & Keppler, H. The origin of the terrestrial noble-gas signature. *Nature* **490**, 531–534 (2012).
34. Rosa, A. D. et al. Krypton storage capacity of the Earth's lower mantle. *Earth Planet Sci. Lett.* **532**, 116032 (2020).
35. Zhu, X., Ye, Y., Smyth, J. R., Liu, D. & Miao, Y. Establishing consistent equations of state for solid noble gases: implication for partitioning behaviors of noble gases in the lower mantle. *Earth Sci. Rev.* **224**, 103872 (2022).
36. Gonnermann, H. M. & Mukhopadhyay, S. Non-equilibrium degassing and a primordial source for helium in ocean-island volcanism. *Nature* **449**, 1037–1040 (2007).
37. Mukhopadhyay, S. & Parai, R. Noble gases: a record of earth's evolution and mantle dynamics. *Annu Rev. Earth Planet Sci.* **47**, 389–419 (2019).
38. Barrat, J. A., Jahn, B. M., Joron, J. L., Auvray, B. & Hamdi, H. Mantle heterogeneity in northeastern Africa: evidence from Nd isotopic compositions and hygromagmaphile element geochemistry of basaltic rocks from the Gulf of Tadjoura and southern Red Sea regions. *Earth Planet Sci. Lett.* **101**, 233–247 (1990).
39. Schilling, J.-G., Kingsley, R. H., Hanan, B. B. & Mccully, B. L. Nd-Sr-Pb isotopic variations along the gulf of aden' evidence for afar mantle plume-continental lithosphere interaction. *J. Geophys. Res.* **97**, 10927–10966 (1992).
40. Mohr, P. & Zanettin, B. *Continental Flood Basalts.* 63–110 (Springer Nature, 1988)
41. Schilling, J.-G. Iceland mantle plume: geochemical evidence along Reykjanes Ridge. *Nature* **242**, 565–571 (1973).
42. Marty, B., Pik, R. & Gezaheg, Y. Helium isotopic variations in Ethiopian plume lavas: nature of magmatic sources and limit on lower mantle contribution. *Earth Planet Sci. Lett.* **144**, 223–237 (1996).
43. Bosworth, W., Huchon, P. & McClay, K. The Red Sea and Gulf of Aden Basins. *J. Afr. Earth Sci.* **43**, 334–378 (2005).
44. Moucha, R. & Forte, A. M. Changes in African topography driven by mantle convection. *Nat. Geosci.* **4**, 707–712 (2011).
45. Koptev, A., Gerya, T., Calais, E., Leroy, S. & Burov, E. Afar triple junction triggered by plume-assisted bi-directional continental break-up. *Sci. Rep.* **8**, 1–7 (2018).
46. Chang, S. J., Merino, M., Van Der Lee, S., Stein, S. & Stein, C. A. Mantle flow beneath Arabia offset from the opening Red Sea. *Geophys. Res. Lett.* **38**, 1–5 (2011).
47. Leroy, S. et al. *From rifting to oceanic spreading in the Gulf of Aden: A synthesis BT - Lithosphere Dynamics and Sedimentary Basins: The Arabian Plate and Analogues* (eds. Al Hosani, K., Roure, F., Ellison, R. & Lokier, S.) 385–427 (Springer Berlin Heidelberg, 2013).
48. Augustin, N., van der Zwan, F. M., Devey, C. W. & Brandsdóttir, B. 13 million years of seafloor spreading throughout the Red Sea Basin. *Nat Commun* **12**, 2427 (2021).
49. Furman, T., Nelson, W. R. & Elkins-Tanton, L. T. Evolution of the East African rift: drip magmatism, lithospheric thinning and mafic volcanism. *Geochim. Cosmochim. Acta* **185**, 418–434 (2016).
50. Williams, C. D., Mukhopadhyay, S., Rudolph, M. L. & Romanowicz, B. Primitive helium is sourced from seismically slow regions in the lowermost mantle. *Geochem. Geophys. Geosyst.* **20**, 4130–4145 (2019).
51. Chang, S. J., Kendall, E., Davaille, A. & Ferreira, A. M. G. The evolution of mantle plumes in East Africa. *J. Geophys. Res. Solid Earth* **125**, e2020JB019929 (2020).

52. Conrad, C. P., Steinberger, B. & Torsvik, T. H. Stability of active mantle upwelling revealed by net characteristics of plate tectonics. *Nature* **498**, 479–482 (2013).
53. Civiero, C. et al. Multiple mantle upwellings in the transition zone beneath the northern East-African Rift system from relative P-wave travel-time tomography. *Geochem. Geophys. Geosyst.* **16**, 2949–2968 (2015).
54. Emry, E. L., Shen, Y., Nyblade, A. A., Flinders, A. & Bao, X. Upper mantle earth structure in africa from full-wave ambient noise tomography. *Geochem. Geophys. Geosyst.* **20**, 120–147 (2019).
55. Chang, S. J. & Van der Lee, S. Mantle plumes and associated flow beneath Arabia and East Africa. *Earth Planet Sci. Lett.* **302**, 448–454 (2011).
56. Marty, B. et al. He, Ar, Sr, Nd and Pb isotopes in volcanic rocks from Afar: Evidence for a primitive mantle component and constraints on magmatic sources. *Geochem. J.* **27**, 219–228 (1993).
57. Nelson, W. R. et al. Distinguishing plume and metasomatized lithospheric mantle contributions to post-flood basalt volcanism on the Southeastern Ethiopian Plateau. *J. Petrol.* **60**, 1063–1094 (2019).
58. Pik, R., Marty, B. & Hilton, D. R. How many mantle plumes in Africa? The geochemical point of view. *Chem. Geol.* **226**, 100–114 (2006).
59. Halldórsson, S. A., Hilton, D. R., Scarsi, P., Abebe, T. & Hopp, J. A common mantle plume source beneath the entire East African Rift System revealed by coupled helium-neon systematics. *Geophys. Res. Lett.* **41**, 2304–2311 (2014).
60. Rooney, T. O. et al. Upper mantle pollution during Afar plume-continental rift interaction. *J. Petrol.* **53**, 365–389 (2012).
61. Ferguson, D. J. et al. Melting during late-stage rifting in Afar is hot and deep. *Nature* **499**, 70–73 (2013).
62. Pik, R., Deniel, C., Coulon, C., Yirgu, G. & Marty, B. Isotopic and trace element signatures of Ethiopian flood basalts: Evidence for plume-lithosphere interactions. *Geochim. Cosmochim. Acta* **63**, 2263–2279 (1999).
63. Beccaluva, L., Bianchini, G., Natali, C. & Siena, F. Continental flood basalts and mantle plumes: a case study of the Northern Ethiopian Plateau. *J. Petrol.* **50**, 1377–1403 (2009).
64. Scarsi, P. & Craig, H. Helium isotope ratios in Ethiopian Rift basalts. *Earth Planet Sci. Lett.* **144**, 505–516 (1996).
65. Barrat, J. A., Fourcade, S., Jahn, B. M., Cheminée, J. L. & Capdevila, R. Isotope (Sr, Nd, Pb, O) and trace-element geochemistry of volcanics from the Erta'Ale range (Ethiopia). *J. Volcanol. Geotherm. Res.* **80**, 85–100 (1998).
66. Ayalew, D. et al. Petrogenesis and origin of modern Ethiopian rift basalts: constraints from isotope and trace element geochemistry. *Lithos* **258–259**, 1–14 (2016).
67. Hagos, M., Koeberl, C. & van Wyk de Vries, B. The Quaternary volcanic rocks of the northern Afar Depression (northern Ethiopia): perspectives on petrology, geochemistry, and tectonics. *J. Afr. Earth Sci.* **117**, 29–47 (2016).
68. Castillo, P. R., Liu, X. & Scarsi, P. The geochemistry and Sr-Nd-Pb isotopic ratios of high 3He/4He Afar and MER basalts indicate a significant role of the African Superplume in EARS magmatism. *Lithos* **376–377**, 105791 (2020).
69. Vidal, P. et al. Changes of mantle sources in the course of a rift evolution: the Afar case. *Geophys. Res. Lett.* **18**, 1913–1916 (1991).
70. Zindler, A. & Hart, S. Chemical geodynamics. *Annu Rev. Earth Planet. Sci.* **14**, 493–571 (1986).
71. Stracke, A., Bizimis, M. & Salters, V. J. M. Recycling oceanic crust: quantitative constraints. *Geochem. Geophys. Geosyst.* **4**, 8003 (2003).
72. Thirlwall, M. F. Pb isotopic and elemental evidence for OIB derivation from young HIMU mantle. *Chem. Geol.* **139**, 51–74 (1997).
73. Stracke, A., Hofmann, A. W. & Hart, S. R. FOZO, HIMU, and the rest of the mantle zoo. *Geochem. Geophys. Geosyst.* **6**, Q05007 (2005).
74. van der Zwan, F. M. et al. Hydrothermal activity at the ultraslow- to slow-spreading Red Sea Rift traced by chlorine in basalt. *Chem. Geol.* **405**, 63–81 (2015).
75. Sun, S. S. & McDonough, W. F. Chemical and isotopic systematics of oceanic basalts: Implications for mantle composition and processes. *Geol. Soc. Spec. Publ.* **42**, 313–345 (1989).
76. Arevalo, R. & McDonough, W. F. Chemical variations and regional diversity observed in MORB. *Chem. Geol.* **271**, 70–85 (2010).
77. Volker, F., McCulloch, M. T. & Altherr, R. Submarine basalts from the Red Sea: New Pb, Sr, and Nd isotopic data. *Geophys. Res. Lett.* **20**, 927–930 (1993).
78. Betton, P. J. & Civetta, L. Strontium and neodymium isotopic evidence for the heterogeneous nature and development of the mantle beneath Afar (Ethiopia). *Earth Planet. Sci. Lett.* **71**, 59–70 (1984).
79. Eissen, J. P. et al. Petrology and geochemistry of basalts from the red sea axial rift at 18° north. *J. Petrol.* **30**, 791–839 (1989).
80. Rogers, N. W. The isotope and trace element geochemistry of basalts from the volcanic islands of the southern Red Sea. *Geol. Soc., Lond. Spec. Publ.* **76**, 455–467 (1993).
81. Altherr, R., Henjes-Kunst, F. & Baumann, A. Asthenosphere versus lithosphere as possible sources for basaltic magmas erupted during formation of the Red Sea: constraints from Sr, Pb and Nd isotopes. *Earth Planet Sci. Lett.* **96**, 269–286 (1990).
82. Gale, A., Dalton, C. A., Langmuir, C. H., Su, Y. & Schilling, J. G. The mean composition of ocean ridge basalts. *Geochem. Geophys. Geosyst.* **14**, 489–518 (2013).
83. Moreira, M. & Sarda, P. Noble gas constraints on degassing processes. *Earth Planet Sci. Lett.* **176**, 375–386 (2000).
84. Willbold, M. & Stracke, A. Trace element composition of mantle end-members: implications for recycling of oceanic and upper and lower continental crust. *Geochem. Geophys. Geosyst.* **7**, 1–30 (2006).
85. Hauri, E. H. & Hart, S. R. ReOs isotope systematics of HIMU and EMII oceanic island basalts from the south Pacific Ocean. *Earth Planet Sci. Lett.* **114**, 353–371 (1993).
86. Moreira, M. & Kurz, M. D. Subducted oceanic lithosphere and the origin of the 'high μ' basalt helium isotopic signature. *Earth Planet Sci. Lett.* **189**, 49–57 (2001).
87. Staudacher, T. & Allègre, C. J. Recycling of oceanic crust and sediments: the noble gas subduction barrier. *Earth Planet Sci. Lett.* **89**, 173–183 (1988).
88. Staudigel, H., Plank, T., White, B. & Schmincke, U. Fluxes During Seafloor Alteration of the Basaltic Crust' DSDP Sites have pointed to the AND. *Geophys. Monogr.* **96**, 19–37 (1996).
89. Nelson, W. R., Furman, T., van Keken, P. E., Shirey, S. B. & Hanan, B. B. OsHf isotopic insight into mantle plume dynamics beneath the East African Rift System. *Chem. Geol.* **320–321**, 66–79 (2012).
90. Van der Voo, R., Spakman, W. & Bijwaard, H. Tethyan subducted slabs under India. *Earth Planet Sci. Lett.* **171**, 7–20 (1999).
91. Chang, S. J., Ferreira, A. M. G., Ritsema, J., Van Heijst, H. J. & Woodhouse, J. H. Joint inversion for global isotropic and radiallyanisotropic mantle structure includingcrustal thickness perturbations. *AGU: J. Geophys. Res., Solid Earth* **120**, 4278–4300 (2015).
92. Hosseini, K., Matthews, K. & Tsekhmistrenko, M. *SubMachine*. https://www.earth.ox.ac.uk/~smachine/cgi/index.php (2023).
93. Saccani, E. et al. New insights into the geodynamics of Neo-Tethys in the Makran area: Evidence from age and petrology of ophiolites from the Coloured Mélange Complex (SE Iran). *Gondwana Res.* **62**, 306–327 (2018).
94. Kaviani, A. et al. Mantle transition zone thickness beneath the middle east: evidence for segmented tethyan slabs, delaminated lithosphere, and lower mantle upwelling. *J. Geophys. Res. Solid Earth* **123**, 4886–4905 (2018).
95. Bellahsen, N., Faccenna, C., Funiciello, F., Daniel, J. M. & Jolivet, L. Why did Arabia separate from Africa? Insights from 3-D laboratory experiments. *Earth Planet Sci. Lett.* **216**, 365–381 (2003).

96. Houseman, G. A. & Gubbins, D. Deformation of subducted oceanic lithosphere. *Geophys. J. Int.* **131**, 535–551 (1997).
97. Kaufmann, G. & Lambeck, K. Glacial isostatic adjustment and the radial viscosity profile from inverse modeling. *J. Geophys. Res. Solid Earth* **107**, ETG 5-1–ETG 5-15 (2002).
98. Schubert, G., Froidevaux, C. & Yuen, D. A. Oceanic lithosphere and asthenosphere: thermal and mechanical structure. *J. Geophys. Res.* **81**, (1976).
99. Young, A. et al. Global kinematics of tectonic plates and subduction zones since the late Paleozoic Era. *Geosci. Front.* **10**, 989–1013 (2019).
100. Butterworth, N. P. et al. Geological, tomographic, kinematic and geodynamic constraints on the dynamics of sinking slabs. *J. Geodyn.* **73**, 1–13 (2014).
101. Van der Meer, D. G., Spakman, W., Van Hinsbergen, D. J. J., Amaru, M. L. & Torsvik, T. H. Towards absolute plate motions constrained by lower-mantle slab remnants. *Nat. Geosci.* **3**, 36–40 (2010).
102. DePaolo, D. J. & Manga, M. Deep origin of hotspots -the mantle plume model. *Science (1979)* **300**, 920–921 (2003).
103. Tauzin, B., Debayle, E. & Wittlinger, G. Seismic evidence for a global low-velocity layer within the Earth's upper mantle. *Nat. Geosci.* **3**, 718–721 (2010).
104. Thompson, D. A. et al. Hydrous upwelling across the mantle transition zone beneath the Afar Triple Junction. *Geochem. Geophys. Geosyst.* **16**, 834–846 (2015).
105. King, S. D., Frost, D. J. & Rubie, D. C. Why cold slabs stagnate in the transition zone. *Geology* **43**, 231–234 (2015).
106. Toksöz, M. N., Minear, J. W. & Julian, B. R. Temperature field and geophysical effects of a downgoing slab. *J. Geophys. Res.* **76**, 1113–1138 (1971).
107. Tan, E., Gurnis, M. & Han, L. Slabs in the lower mantle and their modulation of plume formation. *Geochem., Geophys. Geosyst.* **3**, 1–24 (2002).
108. Schmidt, M., Devey, C. & Eisenhauer, A. *FS Poseidon Fahrtbericht/ Cruise Report P408 [POS408]-The Jeddah Transect; Jeddah-Jeddah, Saudi Arabia, 13.01.−02.03. 2011* (2011).
109. Schmidt, M., Al-Farawati, R., Al-Aidaroos, A. & Kurten, B. eds. *RV PELAGIA Fahrtbericht / Cruise Report 64PE350/64PE351 – JEDDAH-TRANSECT; 08.03. – 05.04.2012 Jeddah - Jeddah, 06.04 − 22.04.2012 Jeddah - Duba*. https://doi.org/10.3289/GEOMAR_REP_NS_5_2013 (2013)
110. Hemleben, Ch., Roether, W. & Stoffers, P. *Östliches Mittelmeer, Rotes Meer, Arabisches Meer – Cruise No. 31, 30 December 1994 – 22 March 1995* (1995).
111. Altherr, R., Henjes-Kunst, F., Puchelt, H. & Baumann, A. Volcanic activity in the Red Sea axial trough - evidence for a large mantle diapir? *Tectonophysics* **150**, 121–133 (1988).
112. Williams, A. J., Stuart, F. M., Day, S. J. & Phillips, W. M. Using pyroxene microphenocrysts to determine cosmogenic 3He concentrations in old volcanic rocks: an example of landscape development in central Gran Canaria. *Quat. Sci. Rev.* **24**, 211–222 (2005).
113. Carracedo, A., Rodés, Smellie, J. L. & Stuart, F. M. Episodic erosion in West Antarctica inferred from cosmogenic 3He and 10Be in olivine from Mount Hampton. *Geomorphology* **327**, 438–445 (2019).
114. Langmuir, C. H., Vocke, R. D. Jr., Hanson, G. N. & Hart, S. R. A general mixing equation with applications to Icelandic basalts. *Earth Planet Sci. Lett.* **37**, 380–392 (1978).
115. Hofmann, A. W. Mantle geochemistry: the message from oceanic magmatism. *Nature* **385**, 219–229 (1997).
116. Hofmann, A. W. & White, W. M. Mantle plumes from ancient oceanic crust. *Earth Planet Sci. Lett.* **57**, 421–436 (1982).
117. Stokes, G. G. On the effect of the internal friction of fluids on the motion of pendulums. *Trans. Camb. Philos. Soc.* **9**, 8–106 (1850).
118. Turcotte, D. & Schubert, G. *Geodynamics* (Cambridge: Cambridge University Press, 2014).
119. Goes, M., Tuana, N. & Keller, K. The economics (or lack thereof) of aerosol geoengineering. *Clim. Change* **109**, 719–744 (2011).
120. Marty, B. & Zimmermann, L. Volatiles (He, C, N, Ar) in mid-ocean ridge basalts: Assesment of shallow-level fractionation and characterization of source composition. *Geochim. Cosmochim. Acta* **63**, 3619–3633 (1999).

Acknowledgements

We thank Luigia Di Nicola for helping with the measurement of helium isotopes. We also acknowledge Godfrey Fitton and Nick Rogers for the discussion of many aspects of this paper and thank Tanya Furman and two anonymous journal reviewers for their useful and constructive comments on early versions. The financial support for U.B.'s PhD and this study was provided by SUERC.

Author contributions

U.B. wrote the manuscript, conceptualised the study, performed He isotope measurements, performed geochemistry and geophysical modelling, interpreted the results and edited the manuscript. F.M.S conceptualised the study, performed He isotope measurements, performed geochemistry modelling, interpreted the results and edited the manuscript. J-A.B. supplied the samples, performed major oxides/trace elements measurements, and edited the manuscript. A.G.G. performed geophysical modelling, interpreted the results and edited the manuscript. F.M.V.D.Z. supplied the samples and edited the manuscript.

Competing interests

The authors declare no competing interests.

Additional information

Supplementary information The online version contains supplementary material available at https://doi.org/10.1038/s43247-024-01675-2.

Correspondence and requests for materials should be addressed to Ugur Balci.

Peer review information *Communications Earth & Environment* thanks the anonymous reviewers for their contribution to the peer review of this work. Primary Handling Editor: Carolina Ortiz Guerrero. A peer review file is available.